ANTIOXIDANTS & REDOX SIGNALING
Volume 16, Number 3, 2012

DOI: 10.1089/ars.2011.4037

ORIGINAL RESEARCH COMMUNICATION

Oxidative Stress, Inflammation, and Autophagic Stress as the Key Mechanisms of Premature Age-Related Hearing Loss in SAMP8 Mouse Cochlea

Julien Menardo,[1,2*] Yong Tang,[1,2*] Sabine Ladrech,[1,2] Marc Lenoir,[1,2] François Casas,[3] Christophe Michel,[1,2] Jérôme Bourien,[1,2] Jérôme Ruel,[1,2] Guy Rebillard,[1,2] Tangui Maurice,[4] Jean-Luc Puel,[1,2] and Jing Wang[1,2]

Abstract

Aims: In our aging society, age-related hearing loss (ARHL) or presbycusis is increasingly important. Here, we study the mechanism of ARHL using the senescence-accelerated mouse prone 8 (SAMP8) which is a useful model to probe the effects of aging on biological processes. ***Results:*** We found that the SAMP8 strain displays premature hearing loss and cochlear degeneration recapitulating the processes observed in human presbycusis (*i.e.,* strial, sensory, and neural degeneration). The molecular mechanisms associated with premature ARHL in SAMP8 mice involve oxidative stress, altered levels of antioxidant enzymes, and decreased activity of Complexes I, II, and IV, which in turn lead to chronic inflammation and triggering of apoptotic cell death pathways. In addition, spiral ganglion neurons (SGNs) also undergo autophagic stress and accumulated lipofuscin. ***Innovation and Conclusion:*** Our results provide evidence that targeting oxidative stress, chronic inflammation, or apoptotic pathways may have therapeutic potential. Modulation of autophagy may be another strategy. The fact that autophagic stress and protein aggregation occurred specifically in SGNs also offers promising perspectives for the prevention of neural presbycusis. *Antioxid. Redox Signal.* 16, 263–274.

Introduction

In industrial countries, age-related hearing loss (ARHL) or presbycusis is a major health problem, with hearing impairment affecting 16% of the adult population, and over half of those over the age of 60 (26). Presbycusis can vary in severity from mild to severe, the more severe forms affecting communication and contributing to social isolation, depression, and possibly dementia. There is a general agreement that cumulative effects of aging on hearing are exacerbated by genetic and environmental factors such as noise or drug exposure. Due to environmental noise and increasing life expectancy, the prevalence of presbycusis is expected to grow dramatically.

Based on observations of temporal bones from patients with presbycusis, Schuknecht (31) proposed classification into three major forms, namely sensory, neural, and strial ARHL, according to the location of damage (sensory epithelium, spiral ganglion, or stria vascularis). Several mouse models have been produced to mimic the different forms of human ARHL (23). While these models exhibit degeneration of the organ of Corti and spiral ganglion neurons (SGNs), damage to the stria vascularis is generally not observed (21–23). Since the incidence of strial presbycusis has been estimated at 30% in humans (31), the lack of stria vascularis injury limits their use

Innovation

To date, only caloric restriction (33) and the overexpression of endogenous caspase inhibitor XIAP (40) or catalase (34) in mice have been shown to modulate ARHL. Our results provide further evidence that targeting oxidative stress, chronic inflammation, or apoptotic pathways, which have been successful following noise- and ototoxic drug exposure (9, 32, 39) may be efficient at preventing ARHL. Another strategy may be the modulation of autophagy, as done with rapamycin fed to extend the lifespan in the mice (11). Our finding that SGN degeneration shares common mechanisms with other neurodegenerative diseases (*i.e.,* autophagic stress and protein aggregation) offers promising perspectives for the prevention of neural presbycusis.

[1]INSERM–UMR 1051, Institut des Neurosciences de Montpellier, Montpellier, France.
[2]Université Montpellier, Montpellier, France.
[3]INRA, UMR 866 Différenciation Cellulaire et Croissance, Montpellier, France.
[4]INSERM U710, Montpellier, France.
*These authors contributed equally to this work.

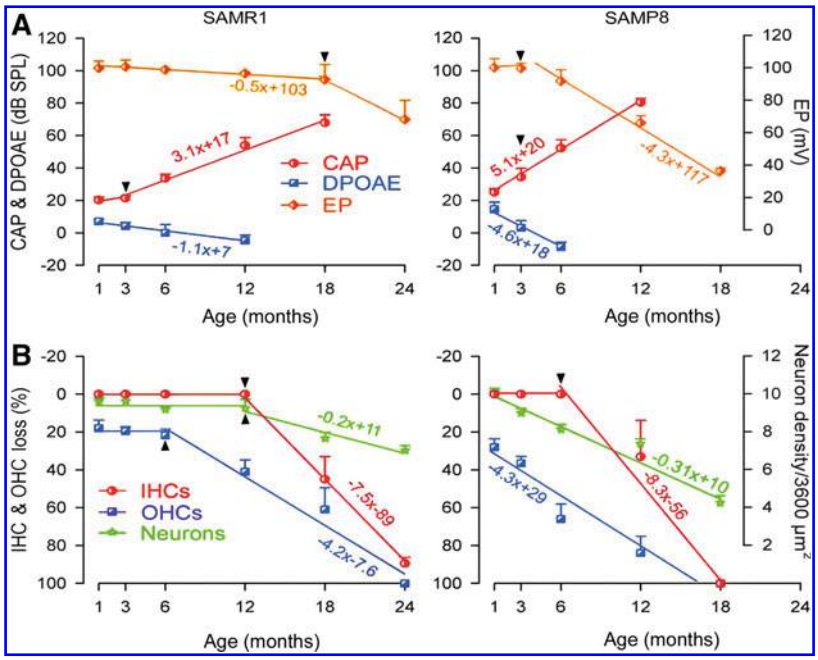

FIG. 1. Functional and morphological assessments in SAMP8 and in SAMR1 mice. **(A)** CAP threshold, DPOAE amplitude evoked by 20 kHz sound stimulations, and EP recordings in SAMR1 and SAMP8 mice. 50 SAMP8 ($n=10$ per age: 1, 3, 6, 12, 18 months) and 60 SAMR1 ($n=10$ per age: 1, 3, 6, 12, 18, 24 months) mice were used for functional assessment. The lifespan of SAMR1 and SAMP8 was approximately 30 and 20 months, respectively. Note the earlier and faster increase in CAP threshold and decrease in DPOAE amplitude and EP value (*arrowheads* indicate broken-stick non-linearities) in the SAMP8. Note that neither CAP threshold nor DPOAEs could be recorded from 18 and 12 months in SAMP8 mice, respectively. **(B)** Age-related loss of IHCs, OHCs, and SGNs. At the end of the functional assessment, the cochleae were removed and prepared for hair cells counting using SEM ($n=5$/age/strain) and SNG counting using light microscopy ($n=5$/age/strain). Note that the number of all cell types, decrease earlier in SAMP8 than in SAMR1: 6 months vs. 12 months for IHCs, earlier than 1 month vs. 6 months for OHCs, and 1 month vs. 12 months for SGNs. (To see this illustration in color the reader is referred to the web version of this article at www.liebertonline.com/ars).

as models of presbycusis. Moreover, the delay in hearing loss in these models entails a thorough investigation over the entire life span of the mouse, which is both labor-intensive and expensive.

The senescence-accelerated mouse strain is derived from AKR/J mice by continuous brother–sister mating selected for a phenotype toward either accelerated senescence or resistance senescence (37). There are nine strains of senescence accelerated prone mice (SAMP) and three strains of senescence-accelerated resistant mice (SAMR). Among these strains, SAMP8 mice have drawn attention for use as models in gerontological research (7).

The present study was designed to study the influence of age on hearing loss in SAMP8 mice. When compared with SAMR1, SAMP8 mice display premature ARHL and cochlear degeneration recapitulating those observed in human presbycusis (*i.e.*, sensory, neural, and strial degeneration). Based on complementary approaches combining biochemistry, and cellular and molecular biology, we show that premature SAMP8 ARHL is due to oxidative stress, alterations of antioxidant enzymes, and decreased activity of Complexes I, II, and IV, which in turn lead to chronic inflammation and triggering of apoptotic cell death pathways. Moreover, autophagic stress and lipofuscin accumulation only accounts for degeneration of SGNs, but not injury of sensory or striatal cells.

Results

Phenotypic description

Age-related functional impairment of hearing. The compound action potential (CAP), reflecting the synchronous activity of the auditory nerve fibers, and distortion product otoacoustic emissions (DPOAEs) which reflect outer hair cell (OHCs) function, showed a predominant high frequency ARHL in both the SAMP8 and SAMR1 mice (Supplementary Fig. S1; Supplementary Data are available online at www.liebertonline.com/ars). The CAP threshold increased and DPOAE decreased 3 months earlier in SAMP8 than in SAMR1 mice at 20 kHz (Fig. 1A).The time course of CAP threshold shift was 1.6 times faster in the SAMP8 strain than in SAMR1 mice (5.1 versus 3.1 dB/month, respectively), with a decrease in DPOAE amplitude occurring 4 times faster (4.6 versus 1.1 dB/month). While the endocochlear potential (EP) generated by the stria vascularis fell dramatically at a rate of 4.3 mV/month between the 3rd (102 mV ± 5.45) and the 18th month (38.3 mV ± 1.66) in SAMP8, it only slightly decreased (0.5 mV/month) in SAMR1.

Morphological correlates. Counting of the sensory hair cells was performed using scanning electron microscopy (SEM, see Supplementary Fig. S2). Loss of sensory hair cells occurred earlier in SAMP8 than in SAMR1 mice [1 vs. 6 months for OHCs, and 6 vs. 12 months for inner hair cells (IHCs)]. However, the time course of degeneration was similar between strains [4.3 vs. 4.2 percentage points (pp)/month for OHCs, and 8.3 vs. 7.5 pp/month for IHCs in SAMP8 and SAMR1, respectively] (Fig. 1B). The measurement of SGN density (Supplementary Fig. S3) revealed earlier (3 vs. 12 months) and more severe degeneration of SGNs in SAMP8 compared to SAMR1. SGN loss reached 60% in SAMP8 versus 20% in SAMR1 by 18 months. The degeneration of SGNs began 6 months before that of IHCs in SAMP8, demonstrating that the loss of SGNs was not secondary to IHC death (Fig. 1B).

Ultrastructural assessments.

Degeneration of the organ of Corti. Transmission electron microscopy (TEM) was used to investigate the status of the hair cells in SAMP8 mice. The hair cells and their innervation

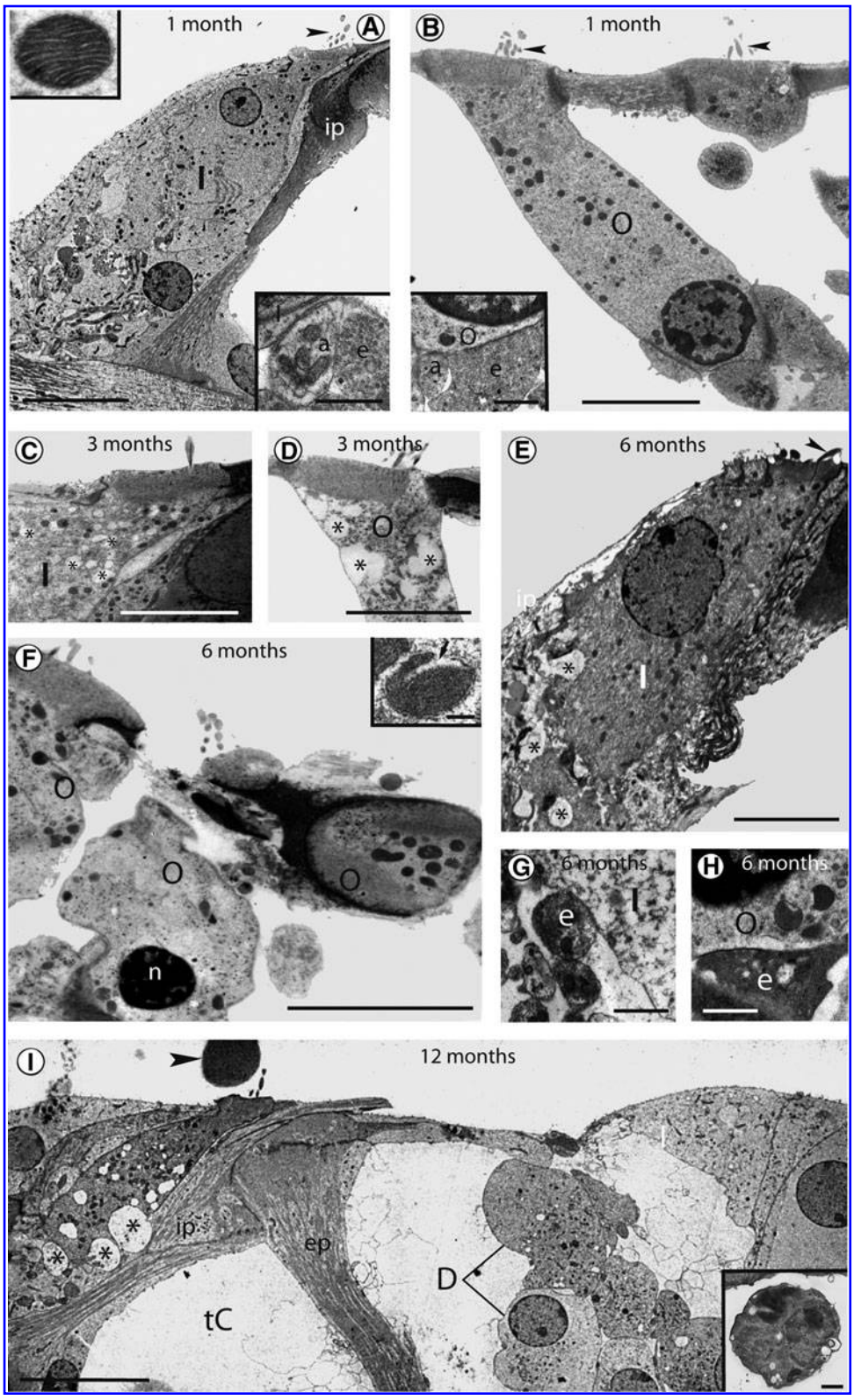

FIG. 2. Ultrastructural analysis of SAMP8 organ of Corti. **(A** and **B)** Normal appearing IHC (I) and OHC (O) at 1 month. *Arrowheads* point to stereociliary bundles. *Lower inset* in **A**: Normal innervation patterns of the IHC, with a synapse between an afferent dendrite (a) and the IHC (I) while a lateral efferent ending (e) contacts the afferent fiber. *Inset* in **B**: Normal innervation below the OHC. Note that a large efferent ending (e) and a small afferent buttons (a) contact the OHC. *Upper inset* in **A**: Normal appearing IHC mitochondria with well-defined cristae. (ip: inner pillar cell). **(C, D)** 3 months. The cytoplasm of both the IHC (in **C**) and the OHC (in **D**) show numerous vacuoles (*asterisks*). **(E–H)** 6 months. **(E)** An IHC with damaged stereocilia (*arrowhead*) and electron-dense cytoplasm. Note the swollen afferent dendrites (*asterisks*) surrounding the IHC basal pole. **(F)** OHCs showing distorted cell bodies and chromatin compaction. One OHC (*right*) is being extruded from the epithelium. *Inset*: A damaged mitochondria with altered cristae and a broken lateral wall (*arrow*). **(G, H)** Abnormal electron-dense efferent terminals contacting an IHC **(G)** and an OHC **(H)**. **(I)** Organ of Corti at 12 months. The OHCs are missing and have been partially replaced by Deiters cells (D). The IHC is vacuolated and the afferent dendrites (*asterisks*) at its basal pole are swollen. Note the apoptotic body floating in the endolymphatic space (*arrowhead*). *Inset*: A macrophage underneath the basilar membrane. (ep: external pillar; tC: tunnel of Corti). Scale bars: **A**–**F** = 10 μm; **G**, **H** = 1 μm; **I** = 20 μm; *Insets* in **A**, **B**, **I** = 1 μm; *Upper Insets* in **B** and **E** = 100 nm. 30 cochleae have been used for TEM analysis (n = 3 per age and per strain).

had a healthy appearance at 1 month (Figs. 2A and 2B, and lower insets of Figs. 2A and 2B). The mitochondria displayed a normal aspect with well defined lamellar cristae (Upper inset Fig. 2A). By 3 months, the IHCs and the OHCs generally showed intracytoplasmic vacuoles (Figs. 2C and 2D). At 6 months, the IHCs generally had an electron dense cytoplasm (Fig. 2E), and the remaining OHCs presented apoptotic condensed cell body and chromatin compaction (Fig. 2F). Mitochondrial cristae were generally undistinguishable and some mitochondria even displayed a broken lateral wall.

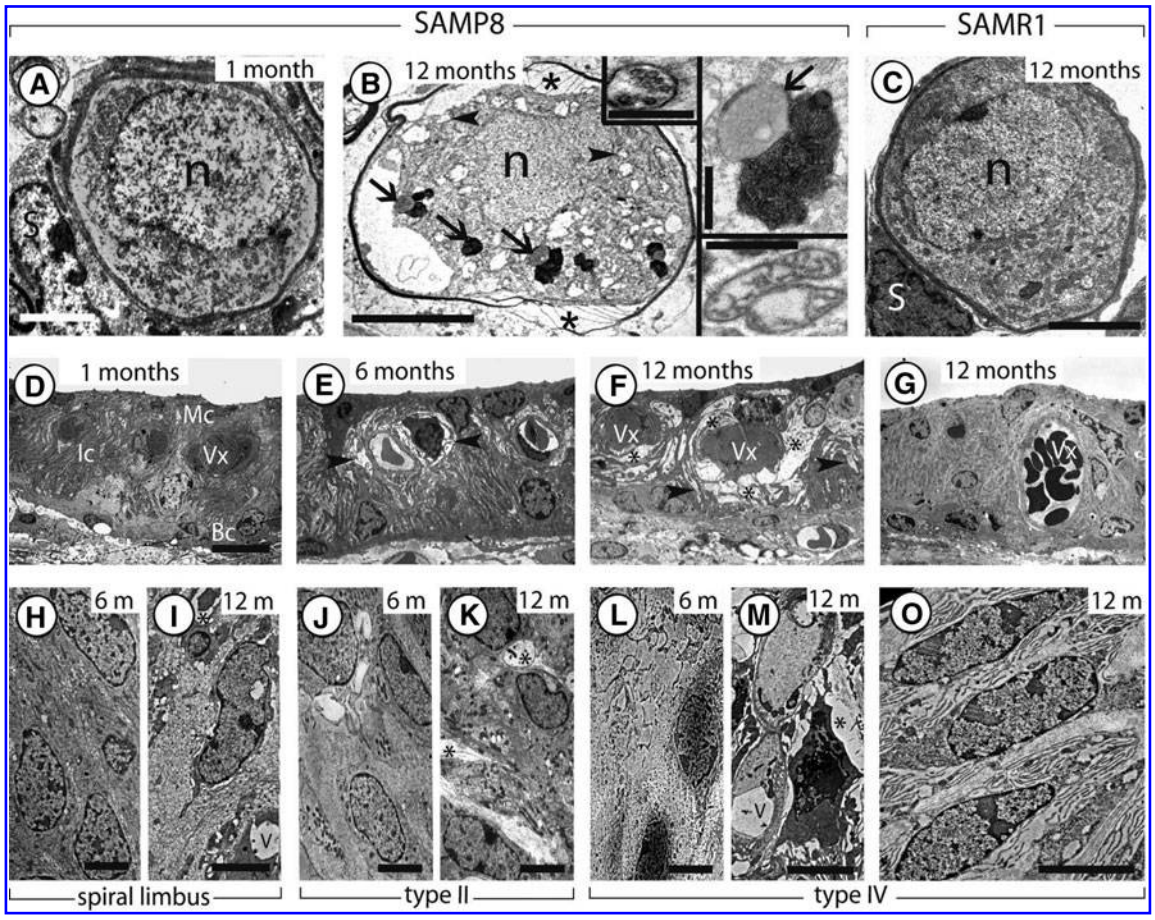

FIG. 3. Ultrastructural analysis of SGNs, stria vascularis, and fibrocytes in SAMP8 (A–B, D–F, H–M) and SAMR1 (C, G, O) SGNs, stria vascularis, and fibrocytes. (**A–C)** SGNs. **(A)** 1 month (SAMP8). Shape and intracellular content of SGNs appear normal (n: SGN nucleus; S: satellite cell). **(B)** 12 months (SAMP8). The SGNs show cell body retraction, a deformed nucleus, cytoplasmic vacuoles, disorganized myelin (*asterisks*), mitochondria with disorganized or absent cristae (*arrowheads*), and electron-dense cytoplasmic inclusions (*arrows*) often associated with a lipid-like droplet. *Upper left inset*: An autophagic vacuole. *Upper right inset*: A dense inclusion with lipid-like droplet. Note the accumulation of membrane lamellae and particles, and the lipid-like droplet (*arrow*). *Lower inset:* Two mitochondria with degenerated cristae, but preserved lateral wall. **(C)** 12 months (SAMR1). The SGNs have a normal appearance with a round nucleus and a homogeneous cytoplasmic content. **(D–G)** stria vascularis. **(D)** (SAMP8) at 1 month, the three layers of strial cells, marginal (Mc), intermediate (Ic), and basal (Bc) cells, and the blood vessels (Vx) appear normal. **(E)** 6 months (SAMP8). Intercellular spaces (*arrowheads*) between intermediate cells are enlarged. **(F)** 12 months (SAMP8). Enlarged intercellular spaces (*arrowheads*) and perivascular edema (*asterisks*) are seen. **(G)** 12 months (SAMR1). The stria vascularis has a normal appearance. **(H–O)** Fibrocytes of the spiral limbus and types II and IV fibrocytes. **(H, J, L)** (SAMP8) at 6 months, all types of fibrocytes appeared normal. **(I, K, M)** 12 months (SAMP8). Intercellular spaces (*asterisks*) are enlarged between the fibrocytes of the spiral limbus and between type II and IV fibrocytes. **(O)** 12 months (SAMR1). Normal appearing type IV fibrocytes. Scale bars: **A**, **B**, **C** = 5 μm; **D–G** = 10 μm; **H–O** = 5 μm. *Insets* = 500 nm. 30 cochleae have been used for TEM analysis ($n = 3$ per age and per strain).

Swollen afferent dendrites surrounded the basal pole of the IHCs (Fig. 2E), and dark efferent terminals were observed under both IHCs (Fig. 2G) and OHCs (Fig. 2H). At 12 months (Fig. 2I), most of the OHCs were lost and the IHCs were profoundly damaged. Between 12 and 18 months, macrophages were visualized within and around (Fig. 2I) the organ of Corti. In SAMR1, the degeneration of the organ of Corti occurred later (after 6 months, not shown).

Degeneration of the spiral ganglion. One-month-old SAMP8 SGNs showed a normal appearance (Fig. 3A). At 12 months, the remaining SGNs showed cell body retraction, cytoplasm vacuolization, and nucleus deformation (Fig. 3B). SGN mitochondria were disorganized with missing cristae (lower inset Fig. 3B). Abundant lipofuscin-like cytoplasmic inclusions containing electron-dense particles often associated with lipid-like droplets were observed in the SGNs (Fig. 3B and upper right inset of Fig. 3B). In addition, characteristic double-membrane-bound autophagic vacuoles were present in the damaged neurons (Upper left inset of Fig. 3B). No damage was observed in SAMR1 SGNs at 12 months (Fig. 3C).

Degeneration of the stria vascularis and fibrocytes. No ultrastructural abnormality was detected in the stria vascularis of 1-month-old SAMP8 mice (Fig. 3D). At age 6 months (Fig. 3E), enlargement of the intercellular spaces of the intermediate cell region occurred, and at 12 months, perivascular edema and enlarged blood vessels were seen in this layer (Fig. 3F). In

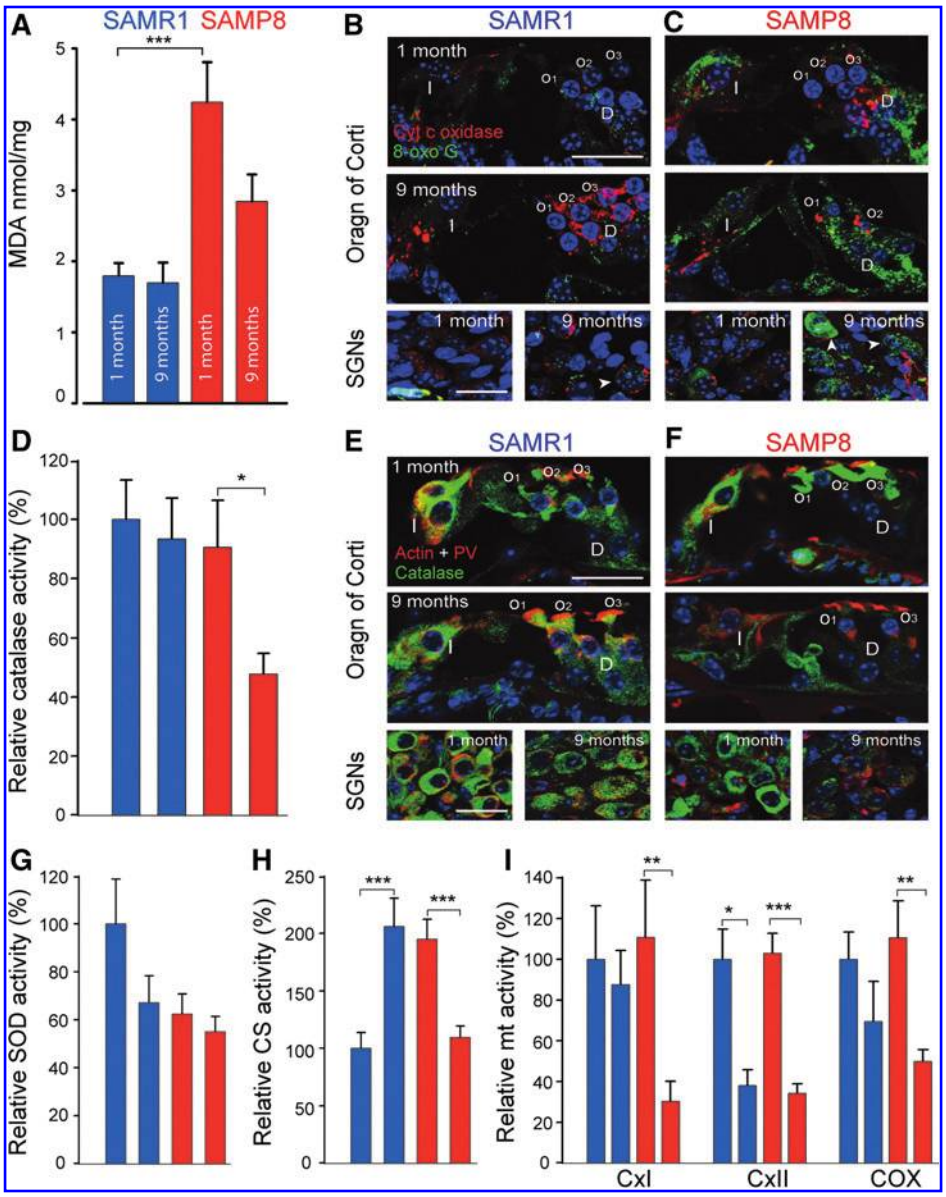

FIG. 4. Oxidative stress, mitochondriogenesis, and mitochondrial bioenergetics. (A, D, G–I) MDA levels **(A)**, catalase **(D)**, SOD **(G)**, CS **(H)**, and complex I(CxI), complex II (CxII), and COX activities **(I)** in whole cochlear extracts from SAMR1 and SAMP8 mice at 1 and 9 months of age ($n=8$ per age and per strain). **(B, C)** Confocal images of transverse cryostat sections of the organ of Corti (*upper and middle panels*) and SGNs (*lower panel*) from SAMR1 **(B)** and SAMP8 **(C)** mice at 1 (*upper and lower left*) and 9 (*middle and lower right*) months ($n=4$ per age and per strain). The sections were labeled for 8-oxoG (*green*), cytochrome c oxidase (*red*), and Hoechst 33342 dye (*blue*). Note the very high density dot-like 8-oxoG staining in the cytoplasm of sensory hair cells, supporting cells, and SGNs of 1 and 9 month-old SAMP8 cochleae **(C)**. At 9 months, some OHCs are missing in SAMP8 organ of Corti (*middle* in **C**). The *arrowheads* (*lower right* in **B** and **C**) indicate the nuclear localization of 8-oxoG. **(E, F)** Confocal images of transverse cryostat sections of the organ of Corti (*upper and middle panels*) and SGNs (*lower panel*) from SAMR1 **(E)** and SAMP8 **(F)** mice at 1 (*upper and lower left*) and 9 (*middle and lower right*) months ($n=4$ per age and per strain). The sections were labeled for catalase (*green*), parvalbumin (*red*), and counter-stained with rhodamine-conjugated phalloidin (*red*) to identify actin and with Hoechst 33342 to label nuclear chromatin (*blue*). Note that one OHC is absent (*middle panel* in **F**) and that the catalase expression is strongly decreased in remaining sensory hair cells and in SGNs (*middle and lower right* in **F**) of 9-month-old SAMP8 cochleae. D, Deiters cells; I, Inner hair cells; O, outer hair cells. Scale bars: Upper and middle images = 35 μm, lower images = 25 μm. (To see this illustration in color the reader is referred to the web version of this article at www.liebertonline.com/ars).

contrast, no strial abnormalities were observed in SAMR1 cochleae at 12 months (Fig. 3G).

Fibrocytes located in the spiral limbus and type II and type IV fibrocytes located in the area of the spiral ligament had a normal appearance in 6-month-old SAMP8 mice (Figs. 3H, 3J, and 3L). Retraction of fibrocyte cell bodies was detected at 12 months (Figs. 3I, 3K, 3M). SAMR1 fibrocytes showed a normal appearance until 12 months (Fig. 3O).

Cellular and molecular mechanisms

Oxidative stress. To determine whether oxidative stress contributed to the ARHL, the levels of malondialdehyde (MDA), a lipid peroxidation product were measured at 1 month (where almost all of the hair cells are present) and at 9 months. MDA levels were significantly higher in 1-month-old SAMP8 cochleae than those in SAMR1 (4.25 ± 0.6 vs. 1.79 ± 0.18 nmol/mg, $p<0.001$, Fig. 4A). At 9 months, although MDA was decreased in SAMP8 cochleae, probably due to the loss of cochlear cells in older cochleae, it remained higher when compared with SAMR1 (2.84 ± 0.38 vs. 1.69 ± 0.28 nmol/mg, $p<0.05$, Fig. 4A). This was then confirmed by confocal microscopy analysis of 7, 8-dihydro-8-oxoguanine (8-oxoG), a key biomarker of oxidative mitochondrial and nuclear DNA damage (38). When compared with 1-month-old SAMR1 cochleae (Upper and lower left Fig. 4B), 1-month-old SAMP8 cochleae exhibited higher density dot-like 8-oxoG staining in the cytoplasm of sensory hair cells, supporting cells, and SGNs, suggesting mitochondrial DNA damage (upper and lower left Fig. 4C). At 9 months, 8-OxoG staining increased in

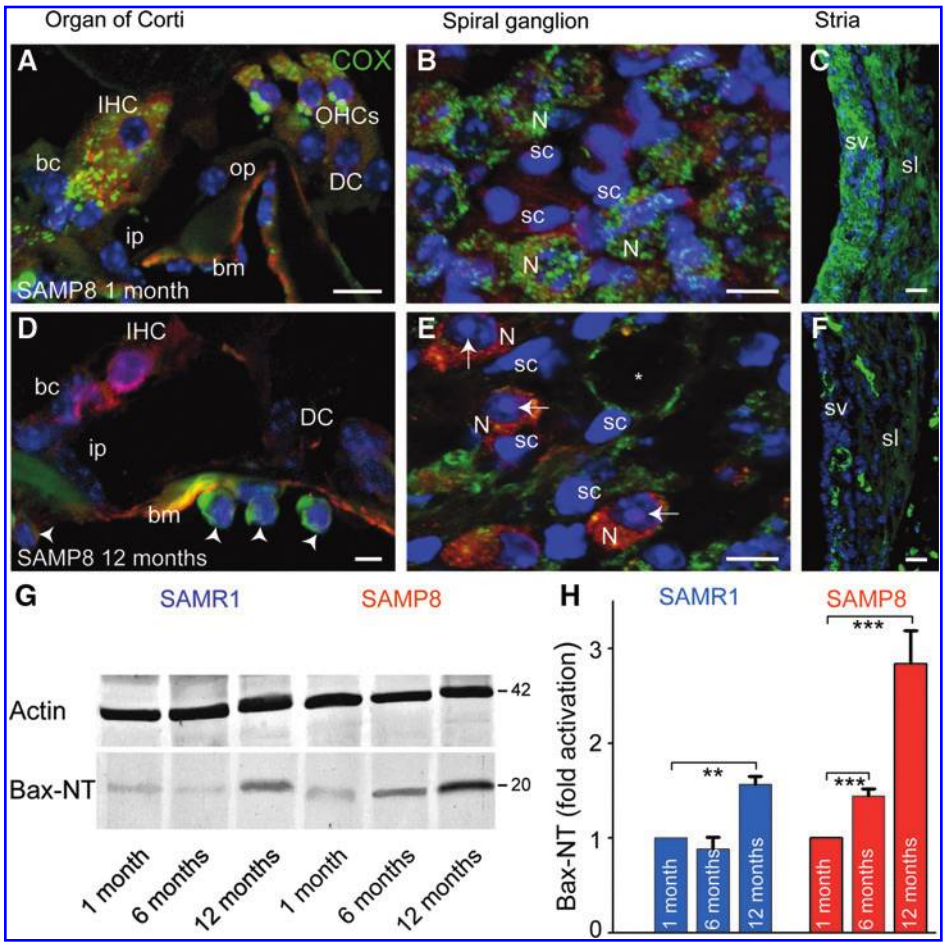

FIG. 5. Cytochrome c oxidase expression and Bax activation. **(A–F)** confocal images of transverse cryostat sections of the organ of Corti **(A, D)**, spiral ganglion **(B, E)** and stria vascularis (sv, in **C**, **F**) from SAMP8 mice at 1 (**A–C**) and 12 months **(D–F)** ($n=4$ per age and per strain). The sections were labeled for cytochrome c oxidase (*green*) and for parvalbumin (*red*) and counter-stained with Hoechst 33342 dye (*blue*). **(A–C)** Normal pattern of intense punctate staining for cytochrome c oxidase in 1-month-old SAMP8. **(D–F)** show decreased or an absence of cytochrome c oxidase staining in 12-month-old SAMP8. Note that the three OHCs (in **D**) and some ganglion neurons (SGNs, in **E**) are absent. The *arrows* (in **E**) indicate the condensed nuclei in the SGNs. The *arrowheads* (in **D**) point to macrophages below the basilar membrane. The *asterisk* (in **E**) indicates a swollen SGN. bc, border cell; bm, basilar membrane, DC, Deiters cells; ip, inner pillar cell; op, outer pillar cell; Sc, satellite cell, sl, spiral ligament. Scale bars: **A–F** = 10 μm. **(G)** Representative Western blots using antibodies to the activated form of Bax (Bax-NT) or β-actin in SAMR1 and SAMP8 at 1, 6, and 12 months. **(H)** Histograms representing the Bax-NT activation in both strains. Data are expressed as level of activation with respect to that in 1-month animals. The cochleae were collected from SAMR1 and SAMP8 mice at 1, 6, and 12 months ($n=7$ per age and per strain). (To see this illustration in color the reader is referred to the web version of this article at www.liebertonline.com/ars).

both strains, with SAMP8 (middle and lower right Fig. 4C) displaying higher levels of staining than SAMR1 (middle and lower right Fig. 4B). In addition, nuclear DNA damage was seen in some SGNs (lower right Figs. 4B and 4C).

Antioxidant functions. Antioxidant enzymes such as catalase and superoxide dismutase (SOD) are recruited to counteract free radical damage. No significant difference was found between the catalase activity measured in 1-month-old SAMR1 cochleae (reference 100% ± 13.2) and that in SAMP8 (90.5% ± 14.8). At 9 months, whilst the catalase activity had been maintained in SAMR1 (93.4% ± 13.9), it was strongly reduced to 47.7 % ± 7.1 in SAMP8 ($p < 0.05$, Fig. 4D). These results were supported by confocal microscopy observations showing very strong catalase expression in the cytoplasm of sensory hair cells, SGNs (upper and lower left Figs. 4E and 4F) and strial cells (not shown) of both strains at 1 month. At 9 months, although the expression remained unchanged in SAMR1 (middle and lower right Fig. 4E), it strongly decreased in SAMP8 (middle and lower right Fig. 4F). Finally SOD activity was lower at 1 month in SAMP8 than in SAMR1 (62.1% ± 8.6 vs. 100% ± 18.6), and further reduced in both strains at 9 months (67.1% ± 11.26 and 55% ± 6.4 respectively, Fig. 4G).

Early mitochondrial dysfunction

Mitochondriogenesis. As a marker of mitochondrial density, we assessed the activity of the enzyme citrate synthase (CS). When compared with 1-month-old SAMR1 (arbitrarily referred to as 100%), CS activity was about 2-fold higher in SAMP8 of the same age (195% ± 17.3, Fig. 4H). Thereafter, the CS activity increased with age in SAMR1 to reach 206% ± 24.8 at 9 months ($p < 0.001$), but it strongly decreased in SAMP8 to reach 109.4% ± 9.9 at the same age ($p < 0.001$). To confirm that the observed increase in CS activity reflected an increased number of mitochondria, we assessed the amount of mitochondrial DNA (mt-DNA). This value was normalized to the relative amount of nuclear DNA. The mt-DNA/nuclear DNA ratio time course correlated with that of CS activity (Supplementary Fig. S4), thus supporting the notion of an overactive mitochondriogenesis in SAMP8 cochlea at young ages.

Mitochondrial bioenergy. To investigate the mechanisms underlying the observed mitochondrial damage, we compared the enzymatic activity of complexes I and II and cytochrome c oxidase (COX) between 1 and 9 months. Here, we report a significant decrease ($p < 0.01$) in complex I activity in SAMP8, but not in SAMR1 mice cochleae (Fig. 4I). In contrast, complex II activity was reduced in both strains (SAMR1:

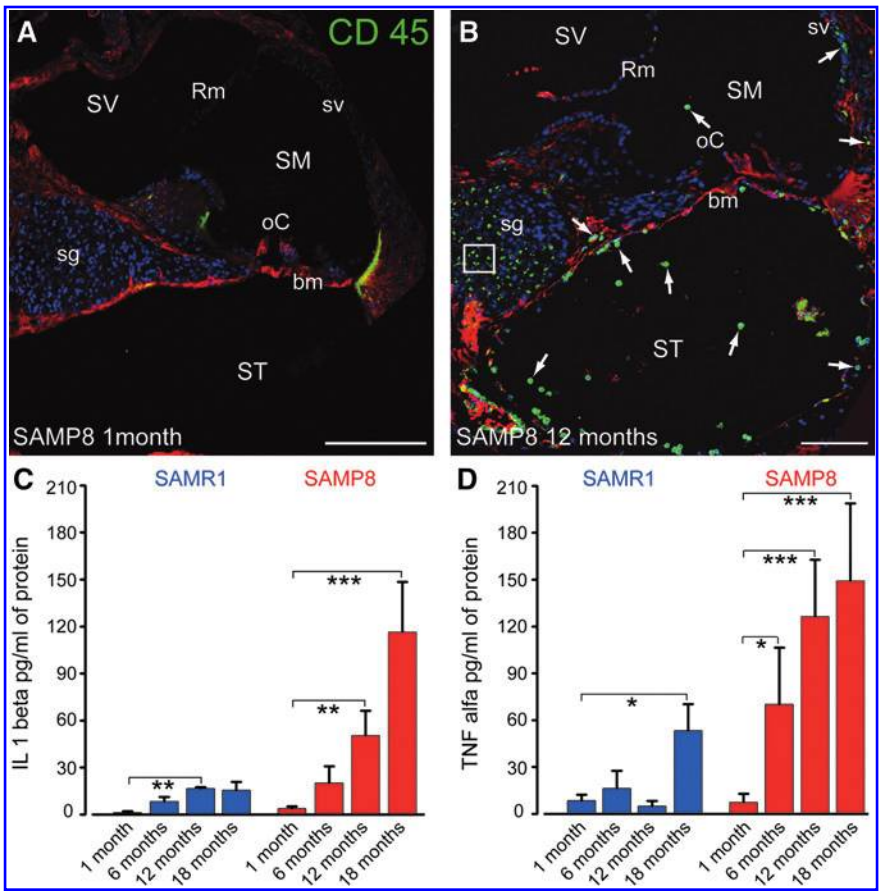

FIG. 6. Macrophages and pro-inflammatory cytokines. (A, B) Confocal images of transverse cryostat sections of the cochleae from SAMP8 mice at 1 month **(A)** and at 12 months **(B)**. The cryostat sections were double-labeled for CD45 (*green*) allowing macrophage identification and for MAP2 (*red*) to identify the hair cell body. Sections were counterstained with Hoechst 33342 to label nuclear chromatin (*blue*). Note that no CD45 (*green*) positive cells were observed in 1-month-old SAMP8 cochleae (in **A**). The CD45 positive cells were seen in the scala tympani (ST), the scala vestibuli (SV), scala media (SM), the basilar membrane (bm), and the stria vascularis (sv) of 12-month-old SAMP8 (in **B**). *White box* focused on lipofuscin granules in the spiral ganglion (sg). oC, organ of Corti; Rm, Reissner's membrane, Scale bar: **A** and **B** = 100 μm. **(C, D)** quantitative analysis of IL-1 beta and TNF-alpha by ELISA. The cochleae were collected from SAMR1 and SAMP8 mice at 1, 6, 12, and 18 months ($n = 4$ per age and per strain). (To see this illustration in color the reader is referred to the web version of this article at www.liebertonline.com/ars).

$p < 0.05$, SAMP8: $p < 0.0009$), making it unlikely to fully account for the premature SAMP8 ARHL. Similarly, both strains showed reduced COX activity, however, this was significantly more marked in SAMP8 ($p < 0.01$, Fig. 4I). The observed reduced COX activity was confirmed by confocal microscopy analysis. One-month-old SAMP8 cochleae exhibited punctuated COX staining in the cytoplasm of sensory hair cells, SGNs, and strial cells (Figs. 5A–5C). At 12 months, this labeling disappeared (Figs. 5D–5F). Note that COX-negative cochlear cells harbored apoptotic condensed nuclei (Fig. 5E).

Apoptotic cell death. To determine whether mitochondrial impairment contributed to the apoptotic cell death, we studied the expression of the pro-apoptotic protein Bax. Western blotting showed a significant increase in levels of Bax expression from as early as 6 months in SAMP8 (Figs. 5G and 5H). The same phenomenon occurred later in SAMR1 mice, at 12 months (Figs. 5G and 5H).

Macrophage invasion and proinflammatory cytokines. An interesting finding was the invasion of cochlear scalae and injured tissues by CD45-positive macrophages (Figs. 5D, 6B). Assessment of proinflammatory cytokine (*i.e.*, TNF-alpha, IL-1β, and IL-6) and anti-inflammatory cytokine (IL-10) levels showed a significant increase in the levels of IL1-β (Fig. 6C) and TNF-alpha (Fig. 6D) from as early as 6 months in SAMP8, while such an increase was only seen in 12- or 18-month-old SAMR1 cochleae.

Autophagic stress. We assessed the level of autophagic stress using the marker microtubule-associated protein light chain 3-II (LC3-II). Cytosolic LC3-I staining was diffuse and uniformly distributed throughout the cytoplasm of cochlear cells in 1-month-old SAMR1 mice: (i.e., detected in the organ of Corti) (Fig. 7A), the spiral ganglion (Fig. 7B), and the stria vascularis (Fig. 7C). In SAMP8 mice, however, an intense and punctuated LC3-II staining was observed as early as 1 month in SGNs (Fig. 7E), but not in the organ of Corti or the stria vascularis (Figs. 7D and 7F). At 6 and 12 months, this punctiform staining increased in the SGNs (Fig. 7H), but remained absent from the organ of Corti (Fig. 7G) and the stria vascularis (Fig. 7I). Western blot semi-quantitative analysis showed that LC3- I expression did not change until 12 months in either strain, when the LC3-II/LC3-I ratio significantly increased in SAMR1 mice. In contrast, an overexpression of LC3-II was seen as soon as the first month in SAMP8 mice, the level of which was maintained until 12 months (Figs. 7J–7K).

Lipofuscin accumulation. Autofluorescent lipofuscin granules were present in the cytoplasm of SGNs (Fig. 8A) from both strains. Quantitative analysis was performed by measuring the ratio of lipofuscin volume/SGN cytoplasm volume. At 1 month, this ratio was significantly higher in SAMP8 compared to SAMR1 (0.8% vs. 0%, $p < 0.05$, Fig. 8B) and significantly increased as early as 6 months (3.8%) reaching 13% at 18 months (Fig. 8B). The age-related increase of lipofuscin total volume in SAMR1 had a slower rate of growth (Fig. 8B). Interestingly, the SGNs containing abundant

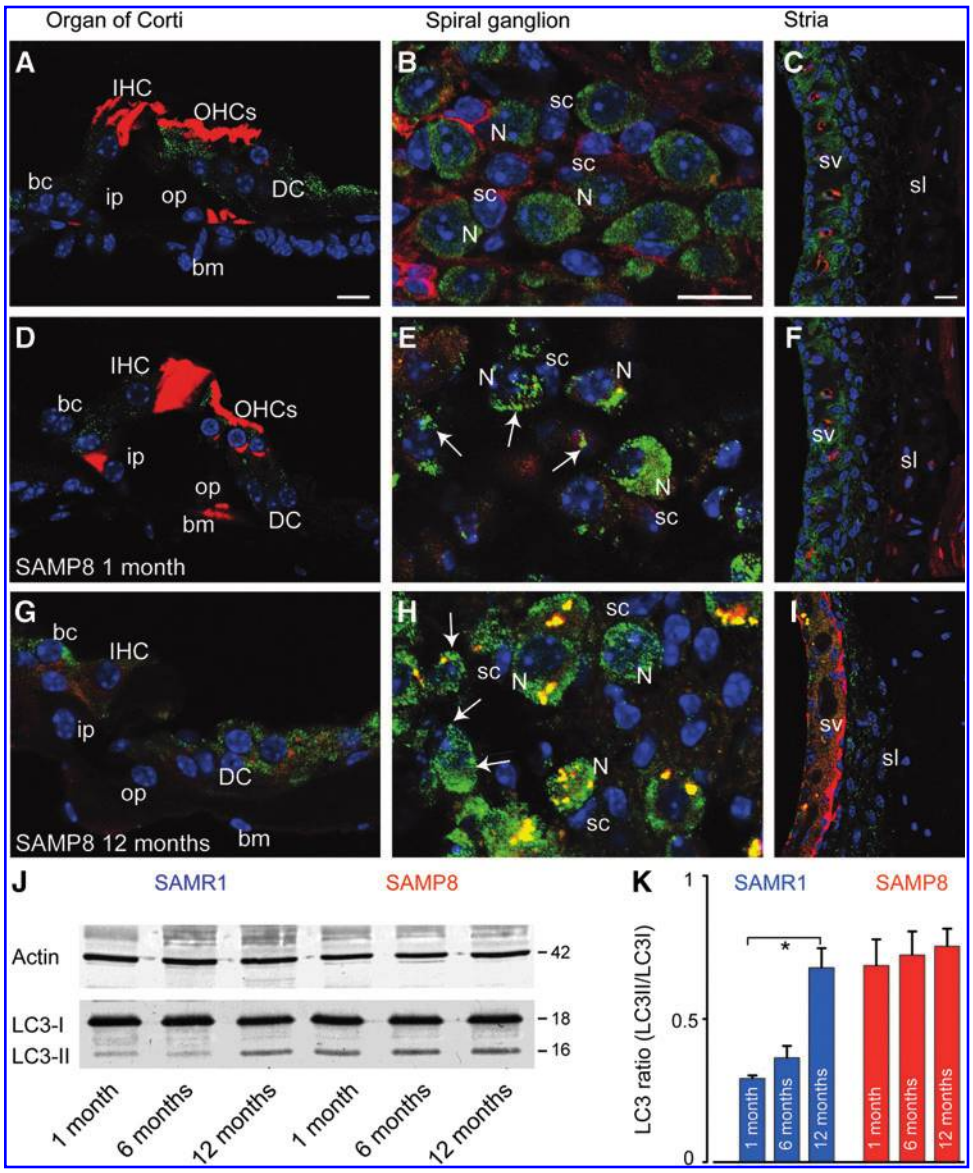

FIG. 7. Autophagic stress in the spiral ganglion neurons. (A–I) Confocal images of cryostat sections of the organ of Corti **(A, D, G)**, spiral ganglion **(B, E, H)** and stria vascularis (Stria, **C**, **F**, and **I**) from 1-month-old SAMR1 (**A--C**) and SAMP8 **(D–F)** and from 12-month-old SAMP8 **(G–I).** The sections were labeled for LC3 (*green*) and counterstained with rhodamine-conjugated phalloidin (*red*) and with Hoechst 33342 (*blue*). **(A–C)** Diffuse pattern of LC3 staining in 1-month-old SAMR1. **(D–I)** diffuse pattern of LC3 staining in the organ of Corti **(D, G)** and the stria **(F, I)**, and punctuate staining for LC3 in the SGNs **(E, H)** in 1-month- **(E)** and 12 month- **(H)** old SAMP8. bc, border cells; bm, basilar membrane; DC, Deiter's cells; ip, inner pillar cells; op: outer pillar cells; sc, satellite cells; sl, spiral ligament. Scale bars: **A**, **D**, and **G** = 50 μm, **B, E, H, C, F, I** = 10 μm. **(J)** Representative western blot using antibodies to the LC3 or β-actin in both strains at 1, 6, and 12 months. **(K)** Histogram representing the change in LC3-II/LC3-I ratio during the aging process in both strains. The cochleae were collected from SAMR1 and SAMP8 mice at 1, 6, and 12 months (n = 7 per age and per strain). (To see this illustration in color the reader is referred to the web version of this article at www.liebertonline.com/ars).

lipofuscin granules generally displayed apoptotic condensed nuclei (Fig. 8A).

Discussion

The SAMP8 strain is a widely used animal model of accelerated senescence and various disorders observed in aging humans (37). Here, we have shown that the SAMP8 strain displays early hearing loss with the sequential degeneration of OHCs, SGNs, stria vascularis, and ultimately IHCs that mimic human presbycusis (31). The pronounced reduction in EP probably results from stria vascularis and fibrocyte damage, as both are involved in the endocochlear cycling of potassium ions (35). The fact that SGN loss occurred before IHC death indicates that degeneration of SGNs is not a consequence of hair cell loss.

Oxidative stress and mitochondrial dysfunction

Oxidative damage in lipid, nucleic acids, and protein has been implicated as a causative factor for a wide variety of age-related diseases (19). In this study, 1-month-old SAMP8 cochleae already exhibit very higher levels of oxidative stress as demonstrated by the overproduction of MDA and 8-oxoG, with the higher level of oxidative damage products being maintained at least up to 9 months. Since the increase of ROS can impair antioxidant function, we also probed the activity of catalase and SOD. Consistent with the study of Wei and collaborators (41) in skin fibroblasts, we found a drastic decline of catalase and SOD activities, and catalase expression in aged SAMP8 cochleae (9 months). Altogether, these results provide strong evidence that oxidative stress contributes to the premature ARHL in SAMP8 mice.

We then probed mitochondriogenesis and found high levels of mt-DNA and CS activity in SAMP8 mice at 1 month, suggesting that the cells attempt to maintain normal respiratory chain activity by strong early stimulation of mitochondriogenesis. Together with the reduced CS activity and levels of mt-DNA in older animals, the decrease in activity levels of complex I, II, and COX also attests to a dramatic impairment of mitochondria function. The decrease of COX activity with

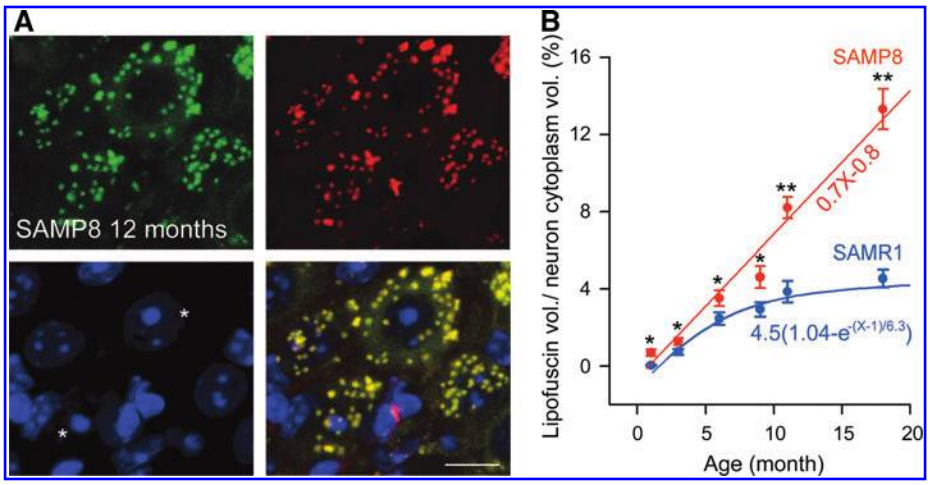

FIG. 8. Lipofuscin accumulation in spiral ganglion neurons. (A) Confocal images of transverse cryostat sections of the SGNs from SAMP8 mice at 12 months. Hoechst 33342 dye was used to label chromatin (*blue*). Note the autofluorescence lipofuscin granules in the cytoplasm of SGNs. The *asterisks* indicate the condensed and pyknotic nuclei (scale bars: A = 10 μm). **(B)** Quantification analysis of lipofuscin accumulation. The ratio of total lipofuscin volume relative to the total neuron cytoplasm volume is plotted as a function of age. In SAMR1, lipofuscin accumulation is approximated with a first-order exponential fit ($R^2 = 0.96$). Note the absence of saturation in SAMP8. Here, the best approximation was a linear fit ($R^2 = 0.95$). The cochleae were collected from SAMR1 and SAMP8 mice at 1, 3, 6, 9, 12, and 18 months ($n = 5$ per age and per strain). (To see this illustration in color the reader is referred to the web version of this article at www.liebertonline.com/ars).

age also fits well with previous data from temporal bone analysis of patients with presbycusis, indicating the high frequency of mutations in the mitochondrial-encoded COX II gene (6). Although the exact cause of altered mitochondrial respiration impairment needs to be elucidated, four unique mt-DNA mutations have been identified in SAM mouse strains (20), suggesting their potential role as a causal factor of premature aging in these strains.

Chronic inflammation

The increase in ROS generation, along with a concomitant disruption in redox balance, may lead to a state of chronic inflammation (12). Indeed, the production of pro-inflammatory cytokines including IL-1, IL-6, and TNF-alpha is greatly influenced by oxidative status (3). Accordingly, we observed higher oxidative stress and drastic decline of catalase and SOD activity in SAMP8 cochleae with a concomitant increase of pro-inflammatory cytokines TNF-alpha and IL-1β. In addition, SAMP8 cochleae show an abundance of macrophages such as that observed in noise- (8, 13) and aminoglycoside- (15) exposed cochleae. This suggests that oxidative stress and chronic inflammation are causal factors triggering premature ARHL in SAMP8 mice.

Autophagic stress and lipofuscin accumulation in SGNs

An important difference between these both strains was the premature occurrence of autophagic stress and lipofuscin accumulation uniquely in the SAMP8 SGNs. This was attested by i) premature higher expression levels of autophagic marker LC3-II, ii) accumulation of damaged mitochondria, iii) autophagic vacuoles, and iv) protein aggregates. Early upregulation of autophagy may serve to remove damaged mitochondria and aberrant proteins induced by oxidative stress and chronic inflammation (17, 25). Indeed, once the pro-survival attempt fails, giant nonfunctional mitochondria and protein aggregates accumulate (10, 30), which in turn may trigger noxious intracellular reactions, including the activation of either apoptotic, autophagic, or both cell death pathways (29). Thus, autophagy may have a dual role in the SGNs: a pro-survival function in young SAMP8 cochleae and an autophagic SGN death function in older animals when it is widely triggered.

Materials and Methods

Animals

The SAMR1 and SAMP8 mice of both sexes were purchased from Harlan SARL Laboratory and housed in a pathogen-free animal care facility. All experiments were conducted according to protocols approved by the «Institut National de la Santé et de la Recherche Medicale» (INSERM) and the French «Ministère de l'Alimentation, de l'Agriculture et de la Pêche».

Functional assessments

Animals were anesthetized by an intraperitoneal injection of a mixture of Rompun 2% (3 mg/kg) and Zoletil 50 (40 mg/kg).

Compound action potential of the auditory nerve. A silver electrode was placed on the round window to record the CAPs evoked by tone bursts (9 msec duration, 1 msec rise/fall, 10/sec). The CAP thresholds (2, 4, 6, 8, 10, 12, 16, 20, 26, and 32 kHz) were defined as the minimum sound intensity necessary to elicit a distinguishable response (27).

Distortion product otoacoustic emissions. The technique used to record DPOAEs has been described in detail elsewhere (27). Briefly, distortions were recorded in the external auditory canal using an ER-10C S/N 2525 probe (Etymotic Research Inc. Elk Grove Village, IL).

Endocochlear potential. A glass microelectrode filled with 0.15 *M* KCl recorded the EP in the scala media of the cochlear basal turn. A silver–silver chloride reference wire was placed in the animal's neck musculature (27).

Morphological assessments

Sensory hair cell counting. Sensory hair cell loss was quantitatively evaluated by counting missing hair cells in apical, middle, and basal regions of the cochlea (24) using SEM (Hitachi S4000). See Supplementary Figure S2 for details.

Spiral ganglion neuron counting. Double blind counting of SGN density in the basal turn was performed within a 3600 μm^2 area of the spiral ganglion under light microscopy (see Supplementary Fig. S3) using a calibrated ocular grid, centered over Rosenthal's canal.

Lipofuscin counting. The counting of lipofuscin in SGNs from the basal turn was performed by quantifying the total volume of lipofuscin relative to the total volume of neuron cytoplasm (see Supplementary Fig. S5 for details).

Ultrastructural analysis. Cochleae were prepared according to a standard protocol for fixation and plastic embedding (15). Ultrathin radial sections of the organ of Corti were observed with TEM (Hitachi 7100).

Molecular assessment

Lipid peroxidation, enzymatic activity, and MtDNA copy number. Cochlear homogenates were prepared as described by Casas (4). Lipid peroxide was estimated by the thiobarbituric acid-reactive substances (TBARS) method as described by Sunderman *et al.* (36) and expressed in nmol/mg MDA. Protein concentration was measured using the Bio-Rad protein assay kit. Complex I, complex II, and COX activities were measured as described previously (14, 28, 42) and expressed in mU/mg protein. CS activity was measured as described by Bergmeyer *et al.* (2). Catalase and SOD activities were measured as described respectively by Beers and Sizer (1) and Marklund (18). Levels of mtDNA were quantified using qPCR (see Supplementary Fig. S5). All experiments were performed in triplicate.

Western blot analysis. Blots were incubated with a rabbit polyclonal antibody against the N-terminal end of Bax protein (1:1000; Upstate Biotechnology, Lake Placid, NY), a rabbit polyclonal antibody against the LC3-I and LC3-II protein (1:500, Sigma-Aldrich, Saint Louis, MO), or a mouse monoclonal antibody against β-actin (1:1000, Sigma-Aldrich), followed by incubation with alkaline phosphatase-conjugated secondary antibody (Sigma Aldrich). All experiments were performed in triplicate. Image scans of Western blots were used for semi-quantitative analysis.

ELISA assay. Levels of proinflammatory cytokines in cochleae were measured using ELISA kits (R&D Systems, Minneapolis, MN). The cochleae were cultured in 96-well plates with modified Dulbecco's modified Eagle's medium in an incubator (37°C, 5% CO_2) for 24 h. The supernatants were then tested for IL-1beta, TNF-alpha, IL-6, and IL-10, using a standard ELISA (5). All experiments were performed in triplicate and reported in pg/ml.

Immunocytochemistry. COX, immune cells, LC3-I and LC3-II, 8-oxoG, and catalase were respectively detected with a mouse anti-cytochrome c oxidase subunit I (1: 500 dilution; Molecular Probes, Eugene OR), a rat monoclonal anti-mouse CD45 (1:100, Chemicon), a rabbit anti-LC3B-I and LC3B-II (1:500, Sigma), a mouse anti-8oxoG-DNA lesion (mouse IGM, 1:500, Santa Cruz, Santa Cruz CA) and a rabbit anti-catalase (1:100, Sigma). A rabbit or mouse anti- parvalbumin (1:500; Swant, Bellinzona, Switzerland) or a mouse anti-MAP2 (1:200, Sigma) were used to label the hair cells and the SGNs (16). Rhodamine-conjugated phalloidin (1:500; Sigma) was used to label actin. All secondary antibodies (Molecular Probes) were used at a dilution of 1:1000. These included an Alexa 488 or 568 donkey anti-mouse IgG, an Alexa 488 or 568 donkey anti-rabbit IgG, an Alexa 488 donkey anti-rat IgG, an Alexa 488 goat anti mouse IGM and an Alexa 594 goat anti mouse IgG. Hoechst 33342 (0.002% wt:vol, Sigma) was used to stain DNA. Fluorescent tags were visualized with a confocal microscope (Leica DMRB). In control specimens without primary antibodies, neither Alexa 488, 568, nor 594 fluorescent tags was observed. Pretreatment with DNase I abolished 8-oxoG fluorescent signal (not shown).

Statistics

Statistics were performed using SigmaPlot software. Functional and morphological data (Fig. 1) were fitted with linear functions. When a unique linear regression curve was not relevant (p-value < 0.05), a broken-stick nonlinearity curve was used. For lipofuscin accumulation data (Fig. 8B), when a linear fit was not suitable to ensure $p < 0.05$, a first-order fitting exponential model was used. All the data are expressed as means ± SEM. Comparison between two samples was performed using paired two-tail *t*-test or Wilcoxon rank test. $^{*}p < 0.05$, $^{**}p < 0.01$, and $^{***}p < 0.001$

Acknowledgments

We thank Dr. Pascale Louis-Plence and Julie Quentin for their help in ELISA analysis. We are grateful to Dr. Régis Nouvian, Dr. Ruth Lloyd, Dr. Carroll Patrick, and Dr. Marci Lesperance for helpful discussions. This study was supported by Fondation de l'Avenir.

Author Disclosure Statement

No competing financial interests exist.

References

1. Beers R and Sizer I. A spectrophotometric method for measuring the breakdown of hydrogen peroxide by catalase, *J Biol Chem* 195: 133–140, 1952.
2. Bergmeyer HU, Gawehen K, and Grassl M. Enzymes as biological reagents. In: New York: Academic Press. 1963, p. 443.
3. Bodamyali T, Stevens CR, Blake DR, and Winyard PG. Reactive oxygen/nitrogen species and acute inflammation: A physiological process. In: *Free Radicals and Inflammation.* Edited by Winyard PG, Blake DR, and Evans CH. Birkha user Verlag, Basel, 2000, pp. 11–16.
4. Casas F, Pessemesse L, Grandemange S, Seyer P, Gueguen N, Baris O, Lepourry L, Cabello G, and Wrutniak-Cabello C. Overexpression of the mitochondrial T3 receptor p43 induces a shift in skeletal muscle fiber types. *PLoS ONE* 3: e2501, 2008.

5. Charbonnier LM, van Duivenvoorde LM, Apparailly F, Cantos C, Han WG, Noël D, Duperray C, Huizinga TW, Toes RE, Jorgensen C, and Louis-Plence P. Immature dendritic cells suppress collagen-induced arthritis by *in vivo* expansion of CD49b+ regulatory T cells. *J Immunol* 177: 3806–3813, 2006.
6. Fischel-Ghodsian N, Bykhovskaya Y, Taylor K, Kahen T, Cantor R, Ehrenman K, Smith R, and Keithley E. Temporal bone analysis of patients with presbycusis reveals high frequency of mitochondrial mutations. *Hear Res* 110: 147–154, 1997.
7. Flood JF and Morley JE. Learning and memory in the SAMP8 mouse. *Neurosci Biobehav Rev* 22: 1–20, 1998.
8. Fujioka M, Kanzaki S, Okano HJ, Masuda M, Ogawa K, and Okano H. Proinflammatory cytokines expression in noise-induced damaged cochlea. *J Neurosci Res* 83: 575–583, 2006.
9. Gabaizadeh R, Staecker H, Liu W, Kopke R, Malgrange B, Lefebvre PP, and Van de Water TR. Protection of both auditory hair cells and auditory neurons from cisplatin induced damage. *Acta Otolaryngol* 117: 232–238, 1997.
10. Grune T, Shringarpure R, Sitte N, and Davies K. Age-related changes in protein oxidation and proteolysis in mammalian cells. *J Gerontol A Biol Sci Med Sci* 56: 459–467, 2001.
11. Harrison DE, Strong R, Sharp ZD, Nelson JF, Astle CM, Flurkey K, Nadon NL, Wilkinson JE, Frenkel K, Carter CS, Pahor M, Javors MA, Fernandez E, and Miller RA. Rapamycin fed late in life extends lifespan in genetically heterogeneous mice. *Nature* 460: 392–395, 2009.
12. Hensley K, Mhatre M, Mou S, Pye QN, Stewart C, West M, and Williamson KS. On the relation of oxidative stress to neuroinflammation: Lessons learned from the G93A-SOD1 mouse model of amyotrophic lateral sclerosis. *Antioxid Redox Signal* 8: 2075- 2087, 2006.
13. Hirose K, Discolo CM, Keasler JR, and Ransohoff R. Mononuclear phagocytes migrate into the murine cochlea after acoustic trauma. *J Comp Neurol* 489: 180–194, 2005.
14. Janssen AJ, Trijbels FJ, Sengers RC, Smeitink JA, van den Heuvel LP, Wintjes LT, Stoltenborg-Hogenkamp BJ, and Rodenburg RJ. Spectrophotometric assay for complex I of the respiratory chain in tissue samples and cultured fibroblasts. *Clin Chem* 53: 729–734, 2007.
15. Ladrech S, Wang J, Simonneau L, Puel JL, and Lenoir M. Macrophage contribution to the response of the rat organ of Corti to amikacin. *J Neurosci Res* 85: 1970–1979, 2007.
16. Ladrech S, Lenoir M, Ruel J, and Puel JL. Microtubule-associated protein 2 (MAP2) expression during synaptic plasticity in the guinea pig cochlea. *Hear Res* 186: 85–90, 2003.
17. Mammucari C and Rizzuto R. Signaling pathways in mitochondrial dysfunction and aging. *Mech Ageing Dev* 131: 536–543, 2010.
18. Marklund S. Spectrophotometric study of spontaneous disproportionation of superoxide anion radical and sensitive direct assay for superoxide dismutase, *J Biol Chem* 251: 7504–7507, 1976.
19. Migliore L and Coppedè F. Environmental-induced oxidative stress in neurodegenerative disorders and aging. *Mutat Res* 674: 73–84, 2009.
20. Mizutani J, Chiba T, Tanaka M, Higuchi K, and Mori M. Unique mutations in mitochondrial DNA of senescence-accelerated mouse (SAM) strains. *J Hered* 92: 352–355, 2001.
21. Ohlemiller KK and Gagnon PM. Cellular correlates of progressive hearing loss in 129S6/SvEv mice. *J Comp Neurol* 469: 377–390, 2004.
22. Ohlemiller KK and Gagnon PM. Apical-to-basal gradients in age-related cochlear degeneration and their relationship to 'primary' loss of cochlear neurons. *J Comp Neurol* 479: 103–116, 2004.
23. Ohlemiller KK. Mechanisms and genes in human strial presbycusis from animal models. *Brain Res* 24: 70–83, 2009.
24. Ou HC, Harding GW, and Bohne BA. An anatomically based frequency-place map for the mouse cochlea. *Hear Res* 145: 123–129, 2000.
25. Philo JS and Arakawa T. Mechanisms of protein aggregation. *Curr Pharm Biotechnol* 10: 348–351, 2009.
26. Pleis JR and Lethbridge-Cejku M. Summary health statistics for U.S. adults: National Health Interview Survey. *Vital Health Stat* 10: 1–153, 2006.
27. Ruel J, Wang J, Demêmes D, Gobaille S, Puel JL, and Rebillard G. Dopamine transporter is essential for the maintenance of spontaneous activity of auditory nerve neurones and their responsiveness to sound stimulation. *J Neurochem* 97: 190–200, 2006.
28. Rustin P, Chretien D, Bourgeron T, Gérard B, Rötig A, Saudubray JM, and Munnich A. Biochemical and molecular investigations in respiratory chain deficiencies. *Clin Chim Acta* 228: 35–51, 1994.
29. Sánchez I, Xu CJ, Juo P, Kakizaka A, Blenis J, and Yuan J. Caspase-8 is required for cell death induced by expanded polyglutamine repeats. *Neuron* 22: 623–633, 1999.
30. Sohal RS and Brunk UT. Lipofuscin as an indicator of oxidative stress and aging. *Adv Exp Med Biol* 266: 17–26, 1989.
31. Schuknecht HF and Gacek MR. Cochlear pathology in presbycusis. *Ann Otol Rhinol Laryngol* 102: 1–16, 1993.
32. Schmitt NC, Rubel EW, and Nathanson NM. Cisplatin-induced hair cell death requires STAT1 and is attenuated by epigallocatechin gallate. *J Neurosci* 29: 3843–3851, 2009.
33. Sebastian C and Mostoslavsky R. SIRT3 in calorie restriction: Can you hear me now? *Cell* 143: 667–668, 2010.
34. Someya S, Xu J, Kondo K, Ding D, Salvi RJ, Yamasoba T, Rabinovitch PS, Weindruch R, Leeuwenburgh C, Tanokura M, and Prolla TA. Age-related hearing loss in C57BL/6J mice is mediated by Bak-dependent mitochondrial apoptosis. *Proc Natl Acad Sci USA* 106: 19432–19437, 2009.
35. Spicer SS and Schulte BA. The fine structure of spiral ligament cells relates to ion return to the stria and varies with place-frequency. *Hear Res* 100: 80–100, 1996.
36. Sunderman FW Jr, Marzouk A, Hopfer SM, Zaharia O, and Reid MC. Increased lipid peroxidation in tissues of nickel chloride-treated rats. *Ann Clin Lab Sci* 15: 229–236, 1985.
37. Takeda T, Hosokawa M, Takeshita S, Irino M, Higuchi K, Matsushita T, Tomita Y, Yasuhira K, Hamamoto H, Shimizu K, Ishii M, and Yamamuro T. A new murine model of accelerated senescence. *Mech Ageing Dev* 17: 183–194, 1981.
38. Tanrikulu S, Doğru-Abbasoğlu S, Ozderya A, Ademoğlu E, Karadağ B, Erbil Y, and Uysal M. The 8-oxoguanine DNA N-glycosylase 1 (hOGG1) Ser326Cys variant affects the susceptibility to Graves' disease. *Cell Biochem Funct* 29: 244–248, 2011.
39. Wang J and Puel JL From cochlear cell death pathways to new pharmacological therapies. *Mini Rev Med Chem* 8: 1006–1019, 2008.
40. Wang J, Menchenton T, Yin S, Yu Z, Bance M, Morris DP, Moore CS, Korneluk RG, and Robertson GS. Over-expression of X-linked inhibitor of apoptosis protein slows presbycusis in C57BL/6J mice. *Neurobiol Aging* 31: 1238–1249, 2010.
41. Wei YH, Lu CY, Wei CY, Ma YS, and Lee HC. Oxidative stress in human ageing and mitochondrial disease-consequences

of defective mitochondrial respiration and impaired antioxidant enzyme system. *Chin J Physiol* 44: 1–11, 2001.
42. Wharton DC and Tzagoloff A. Studies on the electron transfer system. LVII. The near infrared absorption band of cytochrome oxidase. *J Biol Chem* 239: 2036–2041, 1964.

Address correspondence to:
Dr. Jing Wang
INSERM U. 1051
80 rue Augustin Fliche
34295 Montpellier
France

E-mail: jing.wang@inserm.fr

Date of first submission to ARS Central, May 1, 2011; date of final revised submission, September 17, 2011; date of acceptance, September 18, 2011.

Abbreviations Used

ARHL = age-related hearing loss
CAP = compound action potential
COX = cytochrome c oxidase
CS = citrate synthase
DPOAE = distortion product otoacoustic emissions
EP = endocochlear potential
IHCs = inner hair cells
MDA = malondialdehyde
mt-DNA = mitochondrial DNA
OHCs = outer hair cells
8-oxoG = 7, 8-dihydro-8-oxoguanine
SAMP8 = senescence-accelerated mouse prone/8
SAMR1 = senescence-accelerated resistant 1
SEM = scanning electron microscopy
SGNs = spiral ganglion neurons
SOD = superoxide dismutase
TEM = transmission electron microscopy